Cucurbit-Like AIEgenic Polymersomes with Enzyme-Mediated Motility

Shoupeng Cao[1], Hanglong Wu[1], Imke A. B. Pijpers[1], Jingxin Shao[1], Loai K. E. A. Abdelmohsen[1]*, David S. Williams[2]*, and Jan C. M. van Hest[1]**

[1]Bio-Organic Chemistry, Institute for Complex Molecular Systems, Eindhoven University of Technology, P.O. Box 513, 5600 MB Eindhoven, The Netherlands

[2]School of Cellular and Molecular Medicine, University of Bristol, Bristol, UK.

ABSTRACT

Polymersomes that incorporate aggregation-induced emission (AIEgenic) moieties are attractive inherently fluorescent nanoparticles with biomedical application potential for cell/tissue imaging and tracking, as well as photo therapeutics. An intriguing feature that has not been explored yet is their ability to adopt a range of asymmetric morphologies. Structural asymmetry allows nanoparticles to be exploited as active (motile) systems. Here, we present the design and preparation of AIEgenic cucurbit-shaped polymersome nanomotors with enzyme-powered motility. The cucurbit scaffold was constructed *via* morphology engineering of biodegradable fluorescent AIE-polymersomes, followed by functionalization with enzymatic machinery *via* a layer-by-layer self-assembly process. Due to the enzyme-mediated decomposition of chemical fuel on the cucurbit-like nanomotor surface, enhanced directed motion was attained, when compared to the spherical counterparts. These cucurbit-shaped biodegradable AIE-nanomotors provide a promising platform for the development of active delivery systems with potential for biomedical applications.

KEYWORDS: *polymersomes • nanomotors • aggregation-induced emission • morphology engineering • LBL assembly*

Autonomous motion, as found in living systems, has inspired scientists to design and construct artificial nano- and micro-motors with the capacity of converting various sources of energy into motion.[1-3] Nanomotors utilizing chemical/enzymatic reactions or external physical stimuli (*e.g.* light, magnetic fields, and ultrasound) have all been well established.[4-8] These particulate systems, capable of active transportation, are promising entities for a variety of

complex tasks, ranging from environmental remediation to biomedical delivery.[9-14] A prerequisite for propulsion is that the motor structural design should allow for a higher net force on one side of the particle; this can be a result of an asymmetric distribution of the active moieties on the motor scaffold or asymmetry of the scaffold itself.[15, 16] For instance, in our group, we developed bowl-shaped polymersome nanomotors, stomatocytes, from either poly(ethylene glycol)-*b*-poly(styrene) (PEG-*b*-PS) or poly(ethylene glycol)-*b*-poly(D, L-lactide) (PEG-*b*-PDLLA); both of which are propelled *via* the action of catalytic species enclosed in the bowl-shaped cavity.[17-20] To ensure that nanomotors can be applied in a biomedical setting, they should meet a number of requirements.[14, 21] Besides the importance of size control and biocompatibility/biodegradability, they should also be easily functionalized with catalytic entities that are able to utilize naturally available fuel sources for their motion. Furthermore, for most biomedical applications, effective imaging of nanomotors is a prerequisite.[22, 23] This is often achieved by physically loading the nanomotors with fluorescent compounds, for example, the model drug doxorubicin.[24-26] However, this approach is often hampered by low fluorescence, photo-bleaching, and leakage issues.[27, 28] To make the nanomotors more amenable for biomedical applications, they should be equipped with a robust form of fluorescence. We envision that such fluorescence feature can be provided by the concept of aggregation-induced emission (AIE).[29, 30]

AIEgenic (macro)-molecules, upon self-assembly or simply aggregation, display highly stable and bright fluorescence due to the restricted intramolecular motion and decreased non-radiative energy dissipation of the AIEgenic molecules.[31, 32] The integration of the AIE design principles and nanotechnology is recognized as an alternative frontier to approach and solve intrinsic obstacles for conventional fluorescent materials in nanoscience such as low

loading/conjugation efficiency, burst release, aggregation-induced quenching (ACQ), and/or photo-bleaching behavior.[28, 33, 34] For instance, AIEgenic nanomaterials have been demonstrated to be useful as chemical/bio-sensors, cell imaging, and photo-therapeutic agents, outperforming conventional fluorescent modules due to the combined advantageous features of loading capacity, emission brightness, and fluorescence stability.[30, 35] Furthermore, the versatile nature of AIEgenic molecules enables their facile incorporation into a variety of polymeric particles, including polymer vesicles.[36-39]

Recently, we incorporated AIEgenic features in biodegradable polymersomes, with application potential in the biomedical field.[40] Furthermore, by decorating the spherical polymersomes with a hemispherical gold layer, these AIEgenic particles underwent autonomous motion upon irradiation with NIR light.[41, 42] In fact, a synergistic effect could be observed between the presence of the AIEgens and the responsiveness of the particles to irradiation. The intrinsic properties of the AIEgenic polymersomes were also successfully explored in photodynamic therapy. However, this current generation of AIE-polymersome nanomotors has certain drawbacks. To install asymmetry, a gold coating needs to be introduced which requires an additional processing step that has limited scalability. In addition, the motor is powered by an external light source, while for a number of applications a naturally available energy source would be preferential.[15, 43, 44] As such, it would be an important step forward if the AIE-polymersome scaffold itself has an asymmetric shape and can be loaded effectively with enzymes that act on naturally present substrates.

In this paper, we describe a supramolecular strategy to fabricate structure-inherent fluorescent AIE-polymersome nanomotors with a cucurbit-like topology. Such AIE-polymersomes are composed of biodegradable copolymers that are covalently modified with

aggregation-induced emission (AIE) functionality (**Figure 1**). The inherently asymmetric AIE-polymersomes are decorated with a thin polymeric layer *via* a layer-by-layer (LBL) supramolecular assembly approach, during which catalytic machinery (enzymes) are embedded.[16, 45-47] The resulting enzyme-functionalized AIE-polymersomes are capable of transducing chemical energy into motion. The cucurbit morphology of AIEgenic polymersomes was achieved through fine-tuning the osmotically-induced shape transformation of spherical vesicles. This shape transformation process was driven by the influence of salt and solvent compositions on block copolymer packing, as well as membrane thickness and spontaneous surface curvature.[48, 49] The layer-by-layer assembly strategy allowed the decoration of the particles with either the enzyme catalase or urease and did not impact their structure-inherent fluorescent nature or cucurbit-morphology. By conversion of hydrogen peroxide or urea, the cucurbit polymersome-based nanomotors significantly outperformed their spherical counterparts.

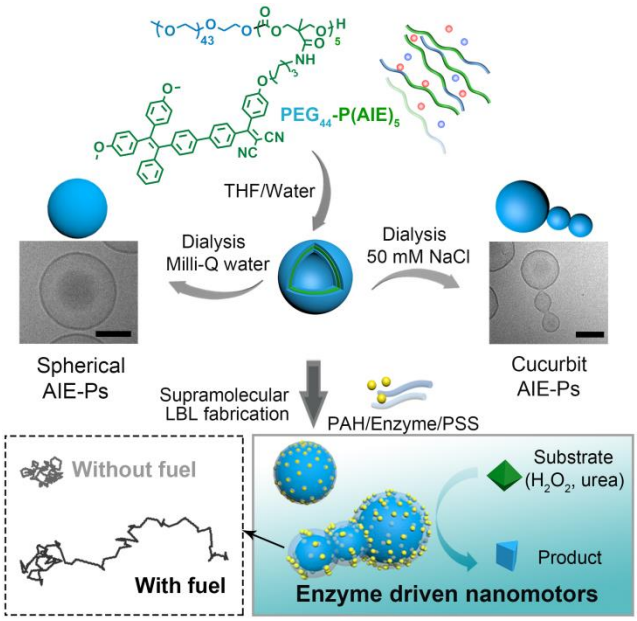

Figure 1. Design of the enzyme-powered cucurbit-shaped AIE-polymersome nanomotors. Top: The molecular structure of the AIEgenic amphiphilic block-co-polymers and self-assembly

following a solvent switch method, whereby a solution of block copolymer in organic solvent (THF) is diluted by water (up to 50% v/v at 0.25 mL h^{-1}). The self-assembly of PEG_{44}-$P(AIE)_5$ block-co-polymer resulted in spherical AIEgenic polymersomes (AIE-Ps) when dialyzed against Milli-Q water, but transformed into cucurbit morphologies in a 50 mM NaCl solution, scale bars = 200 nm. Down: schematic illustration of supramolecular engineering of the cucurbit polymersomes *via* a layer-by-layer assembly approach, in which enzymes (catalase or urease) are effectively embedded in the polyelectrolyte layer (PAH = poly(allylamine hydrochloride); PSS = poly(styrene sulfonate)). Upon addition of substrate (fuel), enzymatic decomposition propels the prepared AIE-polymersome nanomotors, as visualized by analysis of the particle trajectories (in the dashed box).

RESULTS & DISCUSSION

Engineering asymmetric AIE-polymersomes

In order to achieve topological control over AIE-polymersomes with a high degree of asymmetry, a series of block copolymers tagged with AIEgenic moieties were synthesized and their assembly behaviors were subsequently studied and fine-tuned. To this end, utilizing the chemical versatility of poly(trimethylene carbonate) (PTMC) copolymers, well-defined amphiphilic polymers consisting of a poly(ethylene glycol) (PEG) block and an AIEgenic poly(trimethylene carbonate) (PAIE) block comprising both tetraphenylethylene and dicyanovinyl moieties (PEG_{44}-$P(AIE)_n$, $Đ \approx 1.1$) were prepared according to reported procedures (Scheme S1 / S2).[40] Self-assembly of PEG_{44}-$P(AIE)_n$ (where n=5, 8, and 14) was carried out using the well-established solvent switch methodology, in which polymers were

dissolved in a small amount of THF (2 mg mL^{-1} polymer) and after which Milli-Q water (up to 50% vol.) was slowly added using a syringe pump.

Continuous addition of water into the polymer solution decreased the miscibility of block-co-polymers in the water/THF mixture, driving hydrophobic self-assembly. Thereafter, the prepared polymersomes were extensively dialyzed against an aqueous medium for 24 h to remove the organic solvent. After dialysis with Milli-Q water, PEG_{44}-$P(AIE)_{5/8/14}$ copolymers assembled into spherical polymersomes of around 300-500 nm in size with a low polydispersity (PDI $\leqslant$ 0.1), as characterized by dynamic light scattering (DLS) and cryogenic transmission electron microscopy (cryo-TEM) imaging (Figure 2b / S1 / S3 / S5).

Polymersome shape transformation and morphology engineering are inextricably constrained by the self-assembly behavior of copolymers, which is generally recognized to be dictated by geometric, polymer chain entropy effects (relating to the packing parameter), and other kinetic factors.[49-53] This is generally associated with the polymer constituents, fabrication methods, and environmental conditions.[54-56] Previously, we reported that a range of non-spherical polymersome morphologies with anisotropic membranes could be obtained, utilizing an osmotic pressure-based shape transformation strategy to prepare nanotubes and stomatocytes with either PEG-*b*-PS or PEG-*b*-PDLLA block-co-polymer assemblies.[48, 57-59] This was typically realized through deflation of the inner volume and membrane indentation *via* dialysis of the plasticized polymersomes in an organic solvent/water mixture against a water/salt solution. The subsequent osmotic-induced deformation and kinetic trapping resulted in the formation of either prolates (toward tubes) or oblates (toward discs and stomatocytes), directed by the complex interplay between the membrane thickness, headgroup interactions, and spontaneous surface curvature as a result of solvent outflow.[50, 60] To gain insight into the shape transformation of

AIEgenic polymersomes, a number of batches comprising different P(AIE) chain lengths, were dialyzed against aqueous solutions of varying ionic strength [NaCl]. The resulting structures were analyzed using cryogenic transmission electron microscopy (cryo-TEM).

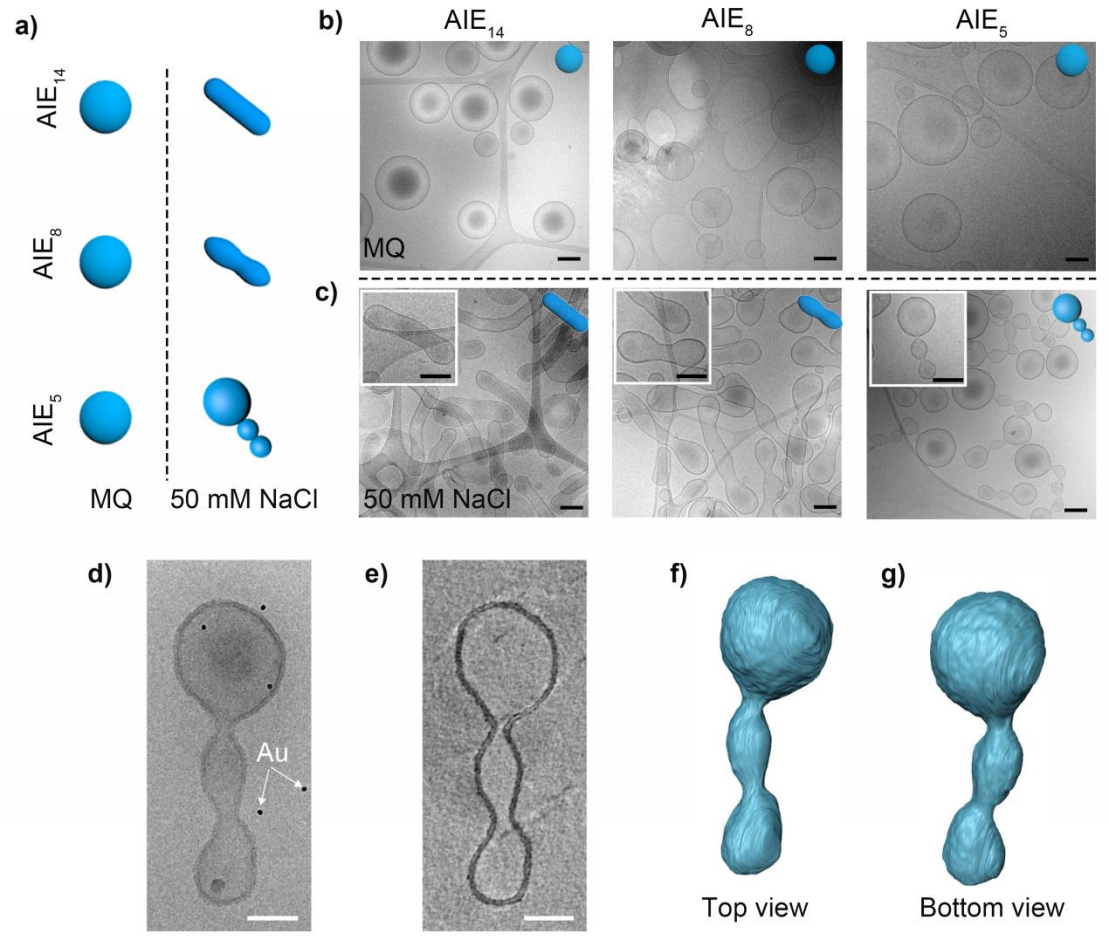

Figure 2. a) Schematic illustration of morphological engineering of AIE-polymersomes bearing different AIE block lengths. b) Cryo-TEM images of PEG_{44}-$P(AIE)_n$ (n=14, 8, 5) polymer assemblies, which remain spherical polymersomes after dialysis against Milli-Q water at 4 ºC. c) While transforming into tubular shaped (n=14), prolate shaped (n=8), and cucurbit shaped (n=5) polymersomes upon dialysis against 50 mM NaCl at 4 ºC. All the scale bars are 200 nm. d) Cryo-TEM image of an individual cucurbit-shaped polymersome. The white arrows point toward fiducially gold nanoparticles. (e-g) Cryo-ET of a cucurbit-shaped polymersome displays its

interior structure and the 3D surface morphology. e) Representative z-slice from the 3D reconstruction of the cucurbit-shaped polymersome showing its cross-sectional morphology. (f-g) Segmented surface rendering of the polymersome from different viewing directions, including the top view (f) and the bottom view (g). Scale bars: 100 nm.

Polymersomes with a flexible membrane in a solvent mixture of THF and Milli-Q water (1:1 v/v) were dialyzed against aqueous solutions with varying salt concentrations at 4 °C. Under such conditions, the glassiness of the membrane structure was retained after removing the organic solvent. It was observed from cryo-TEM imaging that shape transformation process has already occurred after overnight dialysis of PEG_{44}-$P(AIE)_{14}$ polymersomes against 25 mM NaCl, which has resulted in a mixture of morphologies (*i.e.* disc-like (oblate) and elongated nanotubes (prolates)) (Figure S1). Similar results were obtained after overnight dialysis against 50 mM NaCl with (Figure 2c and S1). Interestingly, morphological transitions from spherical polymersomes into bowl-shaped polymersome stomatocytes with wide-open neck, or hexagonally packed hollow hoops, were attained upon dialysis against higher concentrations of NaCl (100 mM and 200 mM, respectively, Figure S1). In addition, the average hydrodynamic size of the PEG_{44}-$P(AIE)_{14}$ polymersomes (as measured by DLS) was significantly reduced after dialysis against NaCl solution (Figure S2) – in line with previous reports demonstrating osmotically induced shape transformation of polymersomes.[20, 48, 58] The PEG_{44}-$P(AIE)_{8}$ AIE-polymersomes with a shorter hydrophobic block showed a distinctly different morphological transformation behavior. For instance, elongated (prolate) nanotubes were observed after dialysis against 25 mM NaCl (Figure S3) whereas, a more uniform distribution of the elongated (prolate) nanotubes was clearly identifiable when dialysis was performed against 50 mM NaCl (Figures 2c and S3). The formation of further elongated nanotubes with increased aspect ratios was achieved

upon dialysis against higher salt solutions (100 and 200 mM NaCl) (Figure S3 and S4). Interestingly, the shape transformation of PEG_{44}-$P(AIE)_5$ polymersomes with an even shorter AIE block resulted in polymersomes with a rarely seen cucurbit-like morphology. This distinct morphological variation was observed upon dialysis against lower concentrations of NaCl (*e.g.* 25 mM, Figure S5). When the dialysis process was performed against 50 mM NaCl, the unusual cucurbit-morphology was predominant (ca. 83%) (Figures 2c and S5). However, dialysis against higher salt solutions (100 mM and 200 mM NaCl) yielded a large ratio of smaller spherical vesicles and only a few cucurbit-shaped vesicles, as confirmed by cryo-TEM analysis (Figure S5). This was further verified by DLS studies, in which the initial spherical polymersomes possessed an average diameter of ca. 500 nm, while dialysis again salt solutions led to sharp size decrease to ~360 nm under 50 mM NaCl condition, and ~230 nm upon dialysis with 200 mM NaCl, respectively (Figure 3a). The effective salt-directed shape transformation into the cucurbit-like AIEgenic polymersomes using 50 mM NaCl was further confirmed by TEM tomographic analysis and 3D tomographic reconstruction (Figures 2d-1g), highlighting this distinct morphology.

When comparing the shape transformation behavior of the polymersomes composed of AIEgenic polymers with different block lengths (5, 8, 14), distinct morphology transition pathways are envisioned. For instance, the formation of PEG_{44}-$P(AIE)_{14}$ polymersome stomatocytes after dialysis against 100 mM NaCl suggests a net negative membrane curvature at these conditions (Figure S1). This can be attributed to an interplay between membrane thickness and high osmotic pressure that induces an outflow of organic solvent from the lumen, at a rate slow enough to maintain anisotropic PEG chain volume (between the interior and exterior surfaces) during the shape transformation process - consistent with literature.[58, 59] When a higher

salt concentration (200 mM NaCl) was applied, formation of hexagonally packed hollow hoops was observed, demonstrating that stomatocytes are possibly the intermediate morphologies that can further evolve into particles with an internal structure by increasing osmotic pressure. Under such hypertonic conditions, the morphology variations of the PEG_{44}-$P(AIE)_{14}$ polymersomes are mainly driven by osmotic energy, which induces their deflation, reduction of the inner volume, PEG anisotropy between the inner and outer surfaces, and membrane indentation.[61] The fact that a heterogeneously mixed fraction of nanotubes and discs was observed when dialyzing with 50 mM NaCl solutions (Figure S1) is complex. At a low concentration of salt (50 mM NaCl), the diffusion of solvent across the thick membrane (*i.e.* solvent outflow) is slower as compared to that at elevated NaCl conditions (*i.e.* 100 and 200 mM). Thus, the 50 mM dialysis conditions generated an anisotropic mismatch between the external and internal membrane surfaces over longer periods of time.[51, 62, 63] In addition, the solvent exchange occurred from organic solvent/water mixture to a salt/water solution such that supramolecular aromatic interactions in the hydrophobic AIE block increased; directly affecting membrane arrangement and anisotropic features.[62] The anisotropic membrane packing during dialysis, as well the π-π aromatic interactions, acted to minimize membrane bending energy, resulting in a mixture of oblates and prolates.[37, 50, 63]

When the degree of hydrophobic AIE units decreases, the PEG_{44}-$P(AIE)_{8}$ polymersomes with a thinner membrane (*e.g.* compared with PEG_{44}-$P(AIE)_{14}$ polymersomes) are then affected by the osmotic pressure in a distinct way. The formation of peanut-like nanotubes was observed from PEG_{44}-$P(AIE)_{8}$ polymersomes upon dialyzing against 50 mM NaCl, indicated that the polymersome adopts a net positive membrane curvature behavior (Figure S3).[48, 58] An increase in osmotic pressure leads to a faster and more complete deflation and higher aspect ratio. Elongated

nanotubes with an apparently increased aspect ratio were observed at 100 mM and 200 mM of NaCl. This can be ascribed to a faster solvent outflow in the presence of a higher osmotic pressure that leads to a geometrical constraint of the surface area during osmosis and a concomitant reduction of internal volume.[48] Since it is understood that the expansion degree of hydrophilic PEG chains is dependent on solvent composition, the pathway by which morphological transformation occurred (in PEG_{44}-$P(AIE)_8$ and PEG_{44}-$P(AIE)_{14}$ polymersomes) was dictated by the membrane thickness and aromatic interactions in the presence of osmotic pressure.[58, 62, 64] This is evident by the fact that under the 100 mM NaCl conditions, stomatocytes were observed with the longer AIE block (*e.g.* $P(AIE)_{14}$), while $P(AIE)_8$ polymer with a shorter block generated nanotubes.

With an even decreased ratio of hydrophobic AIE block and a thinner membrane, the shape transformation of PEG_{44}-$P(AIE)_5$ polymersomes in the presence of [NaCl] during dialysis led to a novel type of morphology not earlier observed for this shape change process. Dialysis against 50 mM NaCl surprisingly resulted in the formation of predominantly a cucurbit-like morphology (Figure 2c / S5). Further analysis *via* TEM tomography and 3D tomographic reconstruction clearly confirmed polymersome 'pearling' process, as well as the open neck structure in the cucurbit-like polymersomes upon dialysis against 50 mM NaCl (Figure 2d-2g). The neck structure formation in the cucurbit polymersomes could be ascribed to the balanced outcome of solvent expulsion, PEG anisotropy, and membrane spontaneous curvature as a result of osmotic pressure. In this case, the short AIE block and thin membrane, with significantly reduced bending energy, are even more easily affected by the osmotic energy, which allows a larger positive membrane curvature than the other blocks, that thus would enable the formation of the budding of the extended prolate structure.[50] The π-π hydrophobic and aromatic interactions

thereby help to maintain membrane rigidity and integrity. In addition, exposure to dialysis solutions with increased salt concentrations (*e.g.* 100 and 200 mM NaCl) gave a significant population of spherical daughter polymersomes with a much smaller size (Figure S5), displaying a fission-like behavior. This supports the pearling process and also indicates that at 50 mM dialysis conditions, the osmotic energy and spontaneous curvature are not able to overcome the free high energy barrier associated with the fission process.[65, 66]

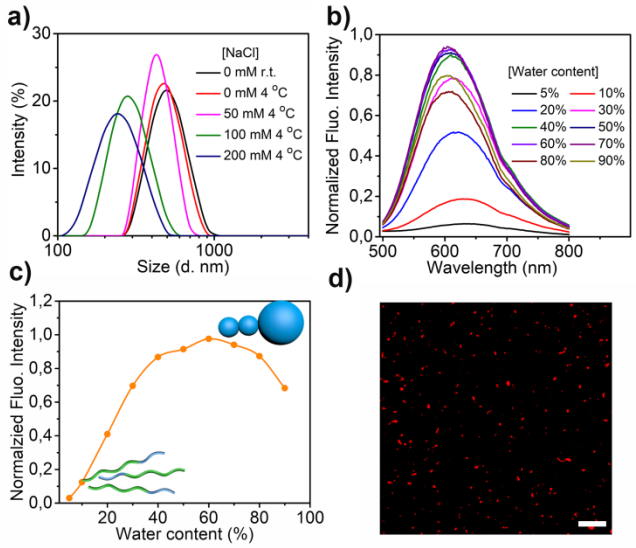

Figure 3. Characterization of cucurbit-like AIE-polymersomes. a) DLS analysis of the size variations of PEG_{44}-$P(AIE)_5$ polymersomes after dialysis with/without salt at room temperature or 4 °C. b) aggregation-induced fluorescence of cucurbit-like polymersomes at different water: DMSO ratios (λ_{ex} = 373 nm / λ_{em} = 617 nm); in DMSO, or at low aqueous content the polymers remained dissolved and did not show emission. c) Normalized fluorescence intensity of PEG_{44}-$P(AIE)_5$ based cucurbit-like AIE-polymersomes when exposed to different DMSO: water ratios (λ_{ex} = 373 nm / λ_{em} = 617 nm). d) Fluorescence characterization of PEG_{44}-$P(AIE)_5$ cucurbit polymersomes using confocal laser scanning microscopy (CLSM), (λ_{ex} = 405 nm / λ_{em} = 600~650 nm), scale bar = 10 μm.

The inherent asymmetric shape of the PEG_{44}-$P(AIE)_5$ cucurbit-like AIE-polymersomes inspired us to use these particles as a chassis for the construction of enzyme-loaded nanomotors. First, the fluorogenic behavior and emission properties of the spherical and cucurbit AIE-polymersomes were assessed by monitoring the fluorescence from the dissolved state in organic solution (DMSO) to the assembled state in the aqueous medium (Figure S6). As displayed in Figures 3b and 3c, a much stronger emission (λ_{ex} = 373 nm / λ_{em} = 617 nm) was detected after the addition of only 20 % aqueous medium compared to the molecularly dissolved state in DMSO. The fluorescence emission was further confirmed using confocal laser scanning microscopy (Figure 3d). In addition, incubation of AIEgenic cucurbit-like polymersomes with FBS or DMEM medium after 24 h did not have a significant impact on their morphology, as verified by SEM imaging (Figure S7), confirming the biological stability of the AIEgenic cucurbit-like polymersomes.

Enzyme decoration of cucurbit-shaped AIE-polymersomes by LBL technique

To realize the fabrication of enzyme-powered cucurbit-shaped AIE-polymersome-based nanomotors, enzymes needed to be included in the design. In a previous approach, enzymes were physically encapsulated in the cavity of polymeric stomatocytes during the shape change process.[20] This approach was not possible for the current system, and the exposure of enzymes to a considerable amount of organic solvent was also less desirable. We, therefore, chose to introduce the enzymes *via* an alternative route. Layer-by-Layer (LBL) self-assembly is a powerful method for the construction of hierarchical materials.[45] A range of functional components, including proteins and enzymes, can be conveniently integrated into LBL systems through non-covalent interactions such as electrostatic, hydrogen bonding, and coordination interactions without the involvement of organic solvent.[16] LBL techniques have also been

applied for the construction of micromotors or multi-compartmentalized systems with enzymatic activity, while also allowing control over the amount of encapsulated enzymes.[41, 46] We, therefore, decided to explore the LBL approach for the construction of enzyme-loaded nanomotor from AIE-polymersomes. To this end, poly(allylamine hydrochloride) (PAH) and poly(styrene sulfonate) (PSS) were alternatingly assembled on the surface of the AIEgenic polymersome template during which urease or catalase was encapsulated *via* strong electrostatic interactions (Figure 1). Surface ζ-potential measurements proved the success of the layer-by-layer assembly that ultimately resulted in enzyme-loaded AIE-polymersomes with a size around 500 nm (Figures 4b and S8). The successful encapsulation of the enzymes (catalase/urea) was further confirmed and quantified by a Bicinchoninic Acid (BCA) protein assay (Figure S8). Notably, scanning electron microscopy (SEM) and cryo-TEM imaging proved that the cucurbit morphology was retained well and not significantly affected during the fabrication and enzyme decoration process, as was also the case for the control spherical counterpart (Figures 4a, 4b and S9). Besides, after removing the polymersome template with THF as a solubilizing solvent, the resulting polyelectrolyte-complex retained its cucurbit morphology, highlighting the robustness of the fabrication approach (Figure S8).

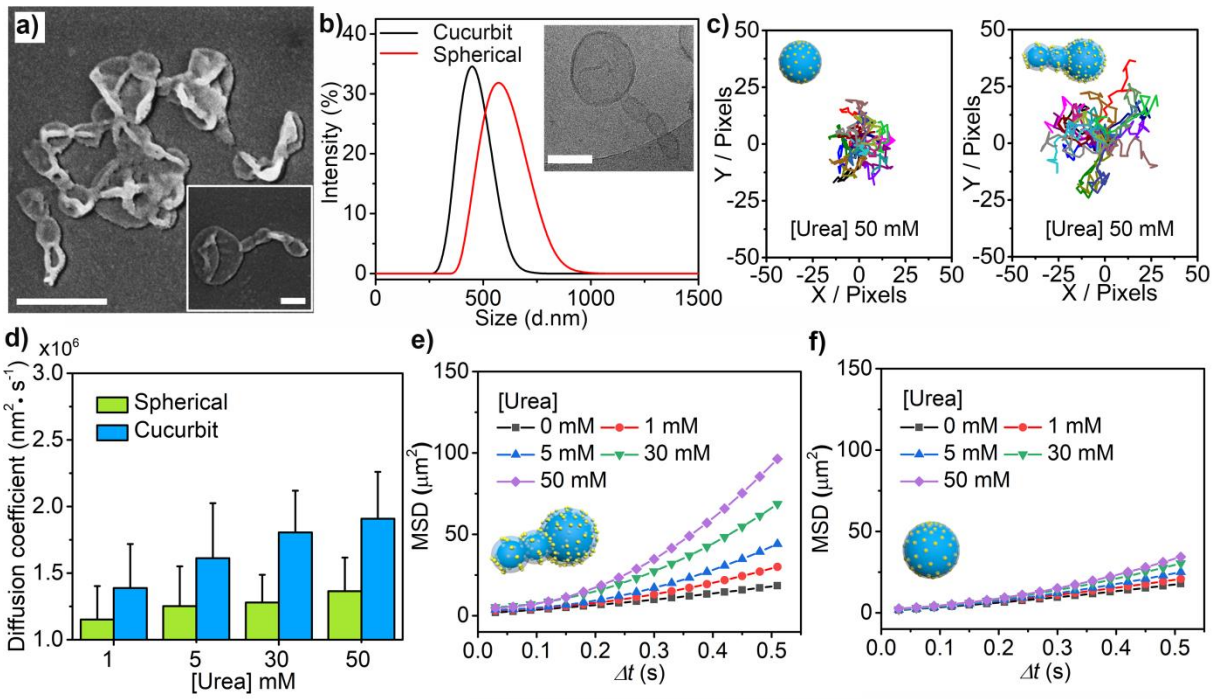

Figure 4. Preparation and characterization of fluorescent polymersome-based enzyme-driven AIE-nanomotors. a) SEM image of as-prepared cucurbit-shaped AIE-polymersome nanomotors. Scale bar = 500 nm; inset scale bar = 200 nm. b) DLS measurements of the spherical and asymmetric AIE-nanomotors after LBL assembly and enzyme loading. Insert is the cryo-TEM image of a cucurbit AIE-nanomotor, scale bar = 200 nm. c) Represented tracking trajectories of spherical and cucurbit-shaped AIE-nanomotors in the presence of 50 mM urea (n=20). d) Diffusion coefficients of spherical and cucurbit-shaped AIE-nanomotors in the presence of urea at varying fuel concentrations. e) Mean squared displacement (MSD) data for cucurbit shaped AIE-nanomotors decorated with urease at varying fuel concentrations, alongside f) MSD data for spherical AIE-nanomotors as control.

Physical properties of nanomotors and motion behavior

The motility of the prepared cucurbit AIE-nanomotors was then investigated in detail. Nanoparticle tracking analysis (NTA) was utilized to record the nanomotors' movement and track their trajectories upon the addition of substrate. The enzyme-mediated motion was first explored with catalase-decorated AIE-nanomotors, which are capable of decomposing hydrogen peroxide (H_2O_2) into water and oxygen.[67] The mean square displacements (MSDs) and velocities of AIE-nanomotors were analyzed using Golestanian's self-diffusiophoretic model (the detailed analysis is described in SI).[68] Cucurbit AIE-nanomotors which were decorated with two layers of the enzyme during LBL assembly, showed the most pronounced MSD values and velocities, which reached ca. 19.8 μm s^{-1} in the presence of 0.75vol% H_2O_2 (Figure S10). Although one would expect linear fits of the MSD curves at relatively high Δt (because of the short rotational diffusion (τ_r) of such small nanoparticles), nonlinear behavior was identified at high concentrations of fuel, which could be ascribed to the bubble generation which counteracts the rapid τ_r (Figure S11).[69] Upon addition of increasing concentrations of substrate, the MSD curves of the cucurbit AIE-nanomotors became parabolic and outperformed their spherical counterparts.

Since in general H_2O_2 is not a biocompatible substrate, urease and urea were employed, as this substrate is naturally present in biological media, including 5−10 mM in human blood and maximally 300 mM in the bladder.[44, 70] Generally, the catalytic reaction that consumes urea in the solution occurring at the surface of the nanomotors will produce a concentration gradient and an active directional flow around the particle surface, resulting in self-generated diffusiophoresis which drives motility.[69] The urease encapsulated in spherical and cucurbit-like AIE-polymersome was observed to display comparable activity (Figure S12). Representative motion videos are recorded and tracking trajectories of the urease decorated AIE-nanomotors before and after exposure to a urea-rich environment are presented (Figure 4c / Video S1-S2). The cucurbit

AIE-nanomotors traveled longer distances after treatment with 50 mM urea than those without urea and the spherical counterparts, indicating that our cucurbit AIE-nanomotors are effectively powered by urea (Figure 4c / S13/ S14). The MSDs at different concentrations of urea as a function of the time interval (Δt) and the diffusion co-efficiencies of such AIE-nanomotors were then analyzed. As the fuel concentration increased, the analyzed MSDs showed an increased value as a result of increasing fuel concentration (Figure 4e). On the other hand, the spherical counterparts as a control displayed a linear fit of the MSD curve even at high concentrations of urea (Figure 4f). In terms of performance, the cucurbit AIE-nanomotors displayed diffusion coefficient values ca. $1.4\sim1.9\times10^6$ $nm^2 \cdot s^{-1}$, depending on the concentration of urea (Figure 4d).

The enhanced diffusion coefficient achieved by cucurbit AIE-nanomotors was up to 45% higher than the spherical control particles (Figure 4d). These results confirm that the cucurbit shape of the AIE-nanomotors and the subsequent non-homogenous enzyme decoration leads to sufficient asymmetry for self-propulsion. Finally, the biocompatibilities of the cucurbit AIE-polymersomes and nanomotors were assessed by using the MTT cell viability assay. Human cervical cancer cells (HeLa cells) were incubated for 24 h with cucurbit AIE-polymersomes and nanomotors at different concentrations. All cells incubated with polymersomes and nanomotors studied displayed >80% cell viability (Figure S15), indicating their excellent biocompatibility. The negligible cytotoxicity of cucurbit-like AIE-polymersome nanomotors enables their application in bio-related domains such as bio-imaging and drug delivery

CONCLUSIONS

In summary, we have constructed AIE-polymersomes with cucurbit morphology by controlling the length of the AIE block and dialysis conditions during the shape change process.

The unusual cucurbit morphology was explored in the construction of AIE-polymersome-based nanomotors. We succeeded in decorating the cucurbit polymersome surface with enzymes using a layer-by-layer assembly strategy. The motile behavior of the AIE-nanomotors was systematically characterized by MSD analysis based on NTA tracking techniques, which demonstrated that the cucurbit motors outperformed their spherical counterparts. This nanomotor design which integrates inherent AIE fluorescence, the vesicular nature of the scaffold, and enzyme-powered motility, provides an interesting platform for the development of nanocarrier systems that can be explored in active transport in a biomedical setting.

METHODS/EXPERIMENTAL

Preparation of spherical AIE-polymersomes. Taking PEG_{44}-$P(AIE)_5$ as an example, in a 4 mL vial, PEG_{44}-$P(AIE)_5$ (1 mg) was dissolved in 0.5 mL of THF and the vial was sealed with a rubber septum. The solution was stirred at 700 rpm for a minimum of 10 minutes prior to the addition of Milli-Q (0.5 mL, 0.25 mL h^{-1}) *via* a syringe pump. A needle was inserted into the septum to release pressure. The resulting cloudy suspension was transferred into a prehydrated dialysis bag (SpectraPor, MWCO: 12-14 kDa, 2 mL cm^{-1}). Dialysis was performed against Milli-Q water at room temperature for 24 hours with a water change after 1 hour. The physicochemical properties of AIE-polymersomes were characterized by dynamic light scatting (DLS), scanning electron microscopy (SEM), and cryo transmission electron microscopy (cryo-TEM).

Shape transformation of AIE-polymersomes. Taking PEG_{44}-$P(AIE)_5$ as an example, in a 4 mL vial, PEG_{44}-$P(AIE)_5$ (1 mg) was dissolved in 0.5 mL of THF and the vial was sealed with a rubber septum. The solution was stirred at 700 rpm for a minimum of 10 minutes prior to the addition of Milli-Q (0.5 mL, 0.25 mL h^{-1}) *via* a syringe pump. A needle was inserted into the

septum to release pressure. The resulting cloudy suspension was transferred into a prehydrated dialysis bag (SpectraPor, MWCO: 12-14 kDa, 2 mL cm^{-1}). Dialysis was performed against different concentration of NaCl at 4 ºC for 24 hours with a water change after 1 hour. The morphology change of AIE-polymersomes was characterized by DLS, SEM, and cryo-TEM.

Preparation of polymersome nanomotors via layer-by-layer approach: In order to construct the enzyme driven AIE-polymersome nanomotors, layer-by-layer self-assembly technique was used for surface modification of the AIE-polymersomes with enzyme layers under mild condition on demand. PAH and PSS solution were prepared at 1 mg mL^{-1} using 0.1 M NaCl solution. For self-assembly via the electrostatic interaction, 1 mL PAH and PSS solution was alternatively added to the AIE polymersome templates (*ca.* 5 mg mL^{-1}) and gently shaken (MS3 shaker, IKA) for 15 min at room temperature. Between different layers, 0.1 M NaCl was used to wash the polymersomes for removing the excess building blocks. Until obtaining the desired assembled layer, the suspension was centrifuged at 10,000 rpm for 5 min to remove all the supernatant, followed by washing with Milli-Q water three times. To encapsulate enzyme, the inner PSS layers were replaced with enzyme solution (2 mg mL^{-1}) and then assembled followed the same procedure. All the samples were stored at 4 ºC before using.

AUTHOR INFORMATION

Corresponding Authors

*Jan C. M. van Hest (j.c.m.v.hest@tue.nl)

*David S. Williams (d.s.williams@bristol.ac.uk)

*Loai K. E. A. Abdelmohsen (l.k.e.a.abdelmohsen@tue.nl)

*Jingxin Shao (j.shao@tue.nl)

Notes

The authors declare no competing financial interests.

ACKNOWLEDGMENT

The authors would like to acknowledge the ERC Advanced Grant Artisym 694120, the Dutch Ministry of Education, Culture and Science (Gravitation program 024.001.035), the NWO-NSFC Advanced Materials (project 792.001.015), and the European Union's Horizon 2020 research and innovation program Marie Sklodowska-Curie Innovative Training Networks Nanomed, (No. 676137) for funding. We thank the Ser Cymru II program for support of DSW; this project received funding from the European Union's Horizon 2020 research and innovation program under the Marie Skłodowska-Curie grant agreement No. 663830. We also thank A. F. Mason for help with Cryo-TEM measurements.

ASSOCIATED CONTENT

The Supporting Information is available free of charge. Included are details of materials, methods, synthesis, and other supporting data utilized in this work.

REFERENCES

(1) Ozin, G. A.; Manners, I.; Fournier-Bidoz, S.; Arsenault, A., Dream Nanomachines. *Adv. Mater.* **2005,** *17*, 3011-3018.

(2) Wang, J., Can Man-Made Nanomachines Compete with Nature Biomotors? *ACS Nano* **2009,** *3*, 4-9.

(3) Palagi, S.; Fischer, P., Bioinspired Microrobots. *Nat. Rev. Mater.* **2018,** *3*, 113-124.

(4) Dey, K. K.; Sen, A., Chemically Propelled Molecules and Machines. *J. Am. Chem. Soc.* **2017,** *139*, 7666-7676.

(5) Xuan, M.; Wu, Z.; Shao, J.; Dai, L.; Si, T.; He, Q., Near Infrared Light-Powered Janus Mesoporous Silica Nanoparticle Motors. *J. Am. Chem. Soc.* **2016,** *138*, 6492-6497.

(6) Xie, H.; Sun, M.; Fan, X.; Lin, Z.; Chen, W.; Wang, L.; Dong, L.; He, Q., Reconfigurable Magnetic Microrobot Swarm: Multimode Transformation, Locomotion, and Manipulation. *Sci. Robot.* **2019,** *4*, eaav8006.

(7) Wang, W.; Wu, Z.; Lin, X.; Si, T.; He, Q., Gold-Nanoshell-Functionalized Polymer Nanoswimmer for Photomechanical Poration of Single-Cell Membrane. *J. Am. Chem. Soc.* **2019,** *141*, 6601-6608.

(8) Liu, L.; Wu, J.; Wang, S.; Kun, L.; Gao, J.; Chen, B.; Ye, Y.; Wang, F.; Tong, F.; Jiang, J.; Ou, J.; Wilson, D. A.; Tu, Y.; Peng, F., Control the Neural Stem Cell Fate with Biohybrid Piezoelectrical Magnetite Micromotors. *Nano Lett.* **2021,** *21*, 3518-3526.

(9) Parmar, J.; Vilela, D.; Villa, K.; Wang, J.; Sánchez, S., Micro- and Nanomotors as Active Environmental Microcleaners and Sensors. *J. Am. Chem. Soc.* **2018,** *140*, 9317-9331.

(10) Li, J.; Esteban-Fernández de Ávila, B.; Gao, W.; Zhang, L.; Wang, J., Micro/Nanorobots for Biomedicine: Delivery, Surgery, Sensing, and Detoxification. *Sci. Robot.* **2017,** *2*, eaam6431.

(11) Wan, M.; Li, T.; Chen, H.; Mao, C.; Shen, J., Biosafety, Functionalities, and Applications of Biomedical Micro/Nanomotors. *Angew. Chem. Int. Ed.* **2021,** *60*, 13158-13176.

(12) Ma, X.; Hahn, K.; Sanchez, S., Catalytic Mesoporous Janus Nanomotors for Active Cargo Delivery. *J. Am. Chem. Soc.* **2015,** *137*, 4976-4979.

(13) Katuri, J.; Ma, X.; Stanton, M. M.; Sánchez, S., Designing Micro- and Nanoswimmers for Specific Applications. *Acc. Chem. Res.* **2017,** *50*, 2-11.

(14) Ou, J.; Liu, K.; Jiang, J.; Wilson, D. A.; Liu, L.; Wang, F.; Wang, S.; Tu, Y.; Peng, F., Micro-/Nanomotors toward Biomedical Applications: The Recent Progress in Biocompatibility. *Small* **2020,** *16*, 1906184.

(15) Wang, H.; Pumera, M., Fabrication of Micro/Nanoscale Motors. *Chem. Rev.* **2015,** *115*, 8704-8735.

(16) Lin, X.; Wu, Z.; Wu, Y.; Xuan, M.; He, Q., Self-Propelled Micro-/Nanomotors Based on Controlled Assembled Architectures. *Adv. Mater.* **2016,** *28*, 1060-1072.

(17) Wilson, D. A.; Nolte, R. J. M.; van Hest, J. C. M., Autonomous Movement of Platinum-Loaded Stomatocytes. *Nat. Chem.* **2012,** *4*, 268-274.

(18) Pijpers, I. A. B.; Cao, S.; Llopis-Lorente, A.; Zhu, J.; Song, S.; Joosten, R. R. M.; Meng, F.; Friedrich, H.; Williams, D. S.; Sánchez, S.; van Hest, J. C. M.; Abdelmohsen, L. K. E. A., Hybrid Biodegradable Nanomotors through Compartmentalized Synthesis. *Nano Lett.* **2020,** *20*, 4472-4480.

(19) Che, H.; Zhu, J.; Song, S.; Mason, A. F.; Cao, S.; Pijpers, I. A. B.; Abdelmohsen, L. K. E. A.; van Hest, J. C. M., Atp-Mediated Transient Behavior of Stomatocyte Nanosystems. *Angew. Chem. Int. Ed.* **2019,** *58*, 13113-13118.

(20) Abdelmohsen, L. K. E. A.; Nijemeisland, M.; Pawar, G. M.; Janssen, G.-J. A.; Nolte, R. J. M.; van Hest, J. C. M.; Wilson, D. A., Dynamic Loading and Unloading of Proteins in Polymeric Stomatocytes: Formation of an Enzyme-Loaded Supramolecular Nanomotor. *ACS Nano* **2016,** *10*, 2652-2660.

(21) Safdar, M.; Khan, S. U.; Jänis, J., Progress toward Catalytic Micro- and Nanomotors for Biomedical and Environmental Applications. *Adv. Mater.* **2018,** *30*, 1703660.

(22) Xu, L.; Mou, F.; Gong, H.; Luo, M.; Guan, J., Light-Driven Micro/Nanomotors: From Fundamentals to Applications. *Chem. Soc. Rev.* **2017,** *46*, 6905-6926.

(23) Yan, X.; Zhou, Q.; Vincent, M.; Deng, Y.; Yu, J.; Xu, J.; Xu, T.; Tang, T.; Bian, L.; Wang, Y.-X. J.; Kostarelos, K.; Zhang, L., Multifunctional Biohybrid Magnetite Microrobots for Imaging-Guided Therapy. *Sci. Robot.* **2017,** *2*, eaaq1155.

(24) Hortelão, A. C.; Patiño, T.; Perez-Jiménez, A.; Blanco, À.; Sánchez, S., Enzyme-Powered Nanobots Enhance Anticancer Drug Delivery. *Adv. Funct. Mater.* **2018,** *28*, 1705086.

(25) Xu, D.; Zhou, C.; Zhan, C.; Wang, Y.; You, Y.; Pan, X.; Jiao, J.; Zhang, R.; Dong, Z.; Wang, W.; Ma, X., Enzymatic Micromotors as a Mobile Photosensitizer Platform for Highly Efficient on-Chip Targeted Antibacteria Photodynamic Therapy. *Adv. Funct. Mater.* **2019,** *29*, 1807727.

(26) Shao, J.; Cao, S.; Williams, D. S.; Abdelmohsen, L. K. E. A.; van Hest, J. C. M., Photoactivated Polymersome Nanomotors: Traversing Biological Barriers. *Angew. Chem. Int. Ed.* **2020,** *59*, 16918-16925.

(27) Chen, M. J.; Yin, M. Z., Design and Development of Fluorescent Nanostructures for Bioimaging. *Prog. Polym. Sci.* **2014,** *39*, 365-395.

(28) Hu, F.; Xu, S.; Liu, B., Photosensitizers with Aggregation-Induced Emission: Materials and Biomedical Applications. *Adv. Mater.* **2018,** *30*, 1801350.

(29) Hong, Y. N.; Lam, J. W. Y.; Tang, B. Z., Aggregation-Induced Emission. *Chem. Soc. Rev.* **2011,** *40*, 5361-5388.

(30) Mei, J.; Leung, N. L. C.; Kwok, R. T. K.; Lam, J. W. Y.; Tang, B. Z., Aggregation-Induced Emission: Together We Shine, United We Soar! *Chem. Rev.* **2015,** *115*, 11718-11940.

(31) Hu, R.; Leung, N. L. C.; Tang, B. Z., Aie Macromolecules: Syntheses, Structures and Functionalities. *Chem. Soc. Rev.* **2014,** *43*, 4494-4562.

(32) Mei, J.; Hong, Y. N.; Lam, J. W. Y.; Qin, A. J.; Tang, Y. H.; Tang, B. Z., Aggregation-Induced Emission: The Whole Is More Brilliant Than the Parts. *Adv. Mater.* **2014,** *26*, 5429-5479.

(33) Feng, G.; Liu, B., Aggregation-Induced Emission (Aie) Dots: Emerging Theranostic Nanolights. *Acc. Chem. Res.* **2018,** *51*, 1404-1414.

(34) Cai, X. L.; Liu, B., Aggregation-Induced Emission: Recent Advances in Materials and Biomedical Applications. *Angew. Chem. Int. Ed.* **2020,** *59*, 9868-9886.

(35) Qian, J.; Tang, B. Z., Aie Luminogens for Bioimaging and Theranostics: From Organelles to Animals. *Chem* **2017,** *3*, 56-91.

(36) Zhang, N.; Chen, H.; Fan, Y.; Zhou, L.; Trépout, S.; Guo, J.; Li, M.-H., Fluorescent Polymersomes with Aggregation-Induced Emission. *ACS Nano* **2018,** *12*, 4025-4035.

(37) Chen, H.; Fan, Y.; Zhang, N.; Trépout, S.; Ptissam, B.; Brûlet, A.; Tang, B. Z.; Li, M.-H., Fluorescent Polymer Cubosomes and Hexosomes with Aggregation-Induced Emission. *Chem. Sci.* **2021,** *12*, 5495-5504.

(38) Zhang, D. P.; Fan, Y. J.; Chen, H.; Trepout, S.; Li, M. H., Co2-Activated Reversible Transition between Polymersomes and Micelles with Aie Fluorescence. *Angew. Chem. Int. Ed.* **2019,** *58*, 10260-10265.

(39) Cao, S.; Xia, Y.; Shao, J.; Guo, B.; Dong, Y.; Pijpers, I. A. B.; Zhong, Z.; Meng, F.; Abdelmohsen, L. K. E. A.; Williams, D. S.; van Hest, J. C. M., Biodegradable Polymersomes with Structure Inherent Fluorescence and Targeting Capacity for Enhanced Photo-Dynamic Therapy. *Angew. Chem. Int. Ed.* **2021,** *60*, 17629-17637.

(40) Cao, S.; Shao, J.; Wu, H.; Song, S.; De Martino, M. T.; Pijpers, I. A. B.; Friedrich, H.; Abdelmohsen, L. K. E. A.; Williams, D. S.; van Hest, J. C. M., Photoactivated Nanomotors *Via* Aggregation Induced Emission for Enhanced Phototherapy. *Nat. Commun.* **2021,** *12*, 2077.

(41) Shao, J.; Abdelghani, M.; Shen, G.; Cao, S.; Williams, D. S.; van Hest, J. C. M., Erythrocyte Membrane Modified Janus Polymeric Motors for Thrombus Therapy. *ACS Nano* **2018,** *12*, 4877-4885.

(42) Xuan, M.; Shao, J.; Gao, C.; Wang, W.; Dai, L.; He, Q., Self-Propelled Nanomotors for Thermomechanically Percolating Cell Membranes. *Angew. Chem. Int. Ed.* **2018,** *57*, 12463-12467.

(43) Hu, J.; Zhou, S.; Sun, Y.; Fang, X.; Wu, L., Fabrication, Properties and Applications of Janus Particles. *Chem. Soc. Rev.* **2012,** *41*, 4356-4378.

(44) Hortelao, A. C.; Simó, C.; Guix, M.; Guallar-Garrido, S.; Julián, E.; Vilela, D.; Rejc, L.; Ramos-Cabrer, P.; Cossío, U.; Gómez-Vallejo, V.; Patiño, T.; Llop, J.; Sánchez, S., Swarming Behavior and in Vivo Monitoring of Enzymatic Nanomotors within the Bladder. *Sci. Robot.* **2021,** *6*, eabd2823.

(45) Xuan, M.; Zhao, J.; Shao, J.; Du, C.; Cui, W.; Duan, L.; Qi, W.; Li, J., Recent Progresses in Layer-by-Layer Assembled Biogenic Capsules and Their Applications. *J. Colloid Interface Sci.* **2017,** *487*, 107-117.

(46) Liu, X.; Formanek, P.; Voit, B.; Appelhans, D., Functional Cellular Mimics for the Spatiotemporal Control of Multiple Enzymatic Cascade Reactions. *Angew. Chem. Int. Ed.* **2017,** *56*, 16233-16238.

(47) De Koker, S.; Hoogenboom, R.; De Geest, B. G., Polymeric Multilayer Capsules for Drug Delivery. *Chem. Soc. Rev.* **2012,** *41*, 2867-2884.

(48) Abdelmohsen, L. K. E. A.; Williams, D. S.; Pille, J.; Ozel, S. G.; Rikken, R. S. M.; Wilson, D. A.; van Hest, J. C. M., Formation of Well-Defined, Functional Nanotubes *Via* Osmotically Induced Shape Transformation of Biodegradable Polymersomes. *J. Am. Chem. Soc.* **2016,** *138*, 9353-9356.

(49) Góźdź, W. T., Spontaneous Curvature Induced Shape Transformations of Tubular Polymersomes. *Langmuir* **2004,** *20*, 7385-7391.

(50) Wong, C. K.; Stenzel, M. H.; Thordarson, P., Non-Spherical Polymersomes: Formation and Characterization. *Chem. Soc. Rev.* **2019,** *48*, 4019-4035.

(51) Mai, Y. Y.; Eisenberg, A., Self-Assembly of Block Copolymers. *Chem. Soc. Rev.* **2012,** *41*, 5969-5985.

(52) Seifert, U.; Berndl, K.; Lipowsky, R., Shape Transformations of Vesicles: Phase Diagram for Spontaneous- Curvature and Bilayer-Coupling Models. *Phys. Rev. A* **1991,** *44*, 1182-1202.

(53) Yuan, H.; Huang, C.; Zhang, S., Dynamic Shape Transformations of Fluid Vesicles. *Soft Matter* **2010,** *6*, 4571-4579.

(54) Varlas, S.; Keogh, R.; Xie, Y.; Horswell, S. L.; Foster, J. C.; O'Reilly, R. K., Polymerization-Induced Polymersome Fusion. *J. Am. Chem. Soc.* **2019,** *141*, 20234-20248.

(55) Blanazs, A.; Madsen, J.; Battaglia, G.; Ryan, A. J.; Armes, S. P., Mechanistic Insights for Block Copolymer Morphologies: How Do Worms Form Vesicles? *J. Am. Chem. Soc.* **2011,** *133*, 16581-16587.

(56) Zhu, Y.; Yang, B.; Chen, S.; Du, J., Polymer Vesicles: Mechanism, Preparation, Application, and Responsive Behavior. *Prog. Polym. Sci.* **2017,** *64*, 1-22.

(57) Men, Y.; Li, W.; Tu, Y.; Peng, F.; Janssen, G.-J. A.; Nolte, R. J. M.; Wilson, D. A., Nonequilibrium Reshaping of Polymersomes *Via* Polymer Addition. *ACS Nano* **2019,** *13*, 12767-12773.

(58) Pijpers, I. A. B.; Abdelmohsen, L. K. E. A.; Williams, D. S.; van Hest, J. C. M., Morphology under Control: Engineering Biodegradable Stomatocytes. *ACS Macro Lett.* **2017,** *6*, 1217-1222.

(59) Kim, K. T.; Zhu, J.; Meeuwissen, S. A.; Cornelissen, J. J. L. M.; Pochan, D. J.; Nolte, R. J. M.; van Hest, J. C. M., Polymersome Stomatocytes: Controlled Shape Transformation in Polymer Vesicles. *J. Am. Chem. Soc.* **2010,** *132*, 12522-12524.

(60) Rikken, R. S. M.; Engelkamp, H.; Nolte, R. J. M.; Maan, J. C.; van Hest, J. C. M.; Wilson, D. A.; Christianen, P. C. M., Shaping Polymersomes into Predictable Morphologies *Via* out-of-Equilibrium Self-Assembly. *Nat. Commun.* **2016,** *7*, 12606.

(61) Salva, R.; Le Meins, J.-F.; Sandre, O.; Brûlet, A.; Schmutz, M.; Guenoun, P.; Lecommandoux, S., Polymersome Shape Transformation at the Nanoscale. *ACS Nano* **2013,** *7*, 9298-9311.

(62) Wong, C. K.; Mason, A. F.; Stenzel, M. H.; Thordarson, P., Formation of Non-Spherical Polymersomes Driven by Hydrophobic Directional Aromatic Perylene Interactions. *Nat. Commun.* **2017,** *8*, 1240.

(63) Wong, C. K.; Martin, A. D.; Floetenmeyer, M.; Parton, R. G.; Stenzel, M. H.; Thordarson, P., Faceted Polymersomes: A Sphere-to-Polyhedron Shape Transformation. *Chem. Sci.* **2019,** *10*, 2725-2731.

(64) Dinç, C. Ö.; Kibarer, G.; Güner, A., Solubility Profiles of Poly(Ethylene Glycol)/Solvent Systems. Ii. Comparison of Thermodynamic Parameters from Viscosity Measurements. *J. Appl. Polym. Sci.* **2010,** *117*, 1100-1119.

(65) Leong, J.; Teo, J. Y.; Aakalu, V. K.; Yang, Y. Y.; Kong, H., Engineering Polymersomes for Diagnostics and Therapy. *Adv. Healthc. Mater.* **2018,** *7*, 1701276.

(66) Kamat, N. P.; Robbins, G. P.; Rawson, J.; Therien, M. J.; Dmochowski, I. J.; Hammer, D. A., A Generalized System for Photoresponsive Membrane Rupture in Polymersomes. *Adv. Funct. Mater.* **2010,** *20*, 2588-2596.

(67) Yang, B.; Chen, Y.; Shi, J., Reactive Oxygen Species (Ros)-Based Nanomedicine. *Chem. Rev.* **2019,** *119*, 4881-4985.

(68) Howse, J. R.; Jones, R. A. L.; Ryan, A. J.; Gough, T.; Vafabakhsh, R.; Golestanian, R., Self-Motile Colloidal Particles: From Directed Propulsion to Random Walk. *Phys. Rev. Lett.* **2007,** *99*, 048102.

(69) Arqué, X.; Romero-Rivera, A.; Feixas, F.; Patiño, T.; Osuna, S.; Sánchez, S., Intrinsic Enzymatic Properties Modulate the Self-Propulsion of Micromotors. *Nat. Commun.* **2019,** *10*, 2826.

(70) Hortelão, A. C.; Carrascosa, R.; Murillo-Cremaes, N.; Patiño, T.; Sánchez, S., Targeting 3d Bladder Cancer Spheroids with Urease-Powered Nanomotors. *ACS Nano* **2019,** *13,* 429-439.

Entry for the Table of Contents